

CFD investigation based on gas burner with low-NO_x strategy of fuel-staging

Yu Zhang, Yuming Xing and Sheng Chen

School of Aviation Science and Engineering, Beihang University, Beijing 100191, China

zhangyu_cn@buaa.edu.cn

Abstract. The 1.1MW burner in a tube furnace of a petrochemical company takes non-premixed fuel-staging as the low-NO_x strategy. The total flow rates of the fuel-gas and air remain the same, however, operating conditions change with different primary/secondary fuel-gas flow rates, whose surrounding flow fields are simulated by the CFD software FLUENT. The outlet fractions of pollutant NO and CO are then obtained, as well as the uniformity of heat transfer from the mixed furnace gas to the tube, thus corresponding to different operating conditions. Finally, this study may help in the selection of practical operating condition.

1. Introduction

As the by-product of combustion, NO is formed in areas of high temperature (usually over 1800K) and high of oxygen fraction [1]. By contrast, CO is the intermediate product that remains in areas with low oxygen fractions. To simultaneously reach the target of low outlet fractions of NO and CO, the strategy of gas-staging with exceeding air is usually adopted; this strategy separates the flame to scatter the high-temperature zone, thereby decreasing the regional high temperature.

Low-NO_x combustion technology is mainly studied experimentally and by numerical computing. Compared with experimental methods, CFD simulation has advantages including shorter cycle, lower cost and reliable result. Chacón et al. [2] carried out a numerical simulation to a traditional gas burner by CFD method, and the result of the study tallied with the experimental data. Improvement schemes were proposed on the base of the CFD computing and outlet NO_x emission decreased dramatically. Bělohradský et al. [3] evaluated influence factors on low-NO_x performance, including burner parameter and operating condition. Liu et al. [4] simulated impact of secondary air on combustion characteristics and NO formation rate in radiation chamber, showing that NO formation rate decreased with increased secondary air flow rate.

In China, industrial tail gas (over 90% of which is NO) is the main source of air pollutant NO_x. The newly-enacted Pollutant Discharge Standard of Petrochemical Industry (GB31571-2015) [5] states that the maximum tail gas fraction of NO_x for a process furnace is 100mg/m³. Moreover, the pollutant CO, which is mainly produced by incomplete combustion, should not be overlooked. Thus, the transformation of burners with exceeding pollutants is imminent.

2. Geometry of the fuel-staging low-NO_x burner and furnace

The burner takes fuel-staging as the low-NO_x strategy. Three primary fuel-gas guns (including one in the middle and two on each side) are located inside the burner refractory brick. Air flows through the bottom of the burner refractory brick, wherein it mixes with primary fuel-gas, and then the primary



combustion takes place. Three secondary fuel-gas guns (including one in the middle and two on each side) are located outside the burner refractory brick. The flue gas after primary combustion, which includes residue oxygen, is mixed with the secondary fuel-gas, and then the secondary combustion takes place. The burner is installed next to the furnace wall, whereas the furnace tube, which absorbs heat, is on the other side. Figure 1 illustrates the geometry of the burner refractory brick, fuel-gas guns, furnace inner wall and furnace tube, as well as their respective positions.

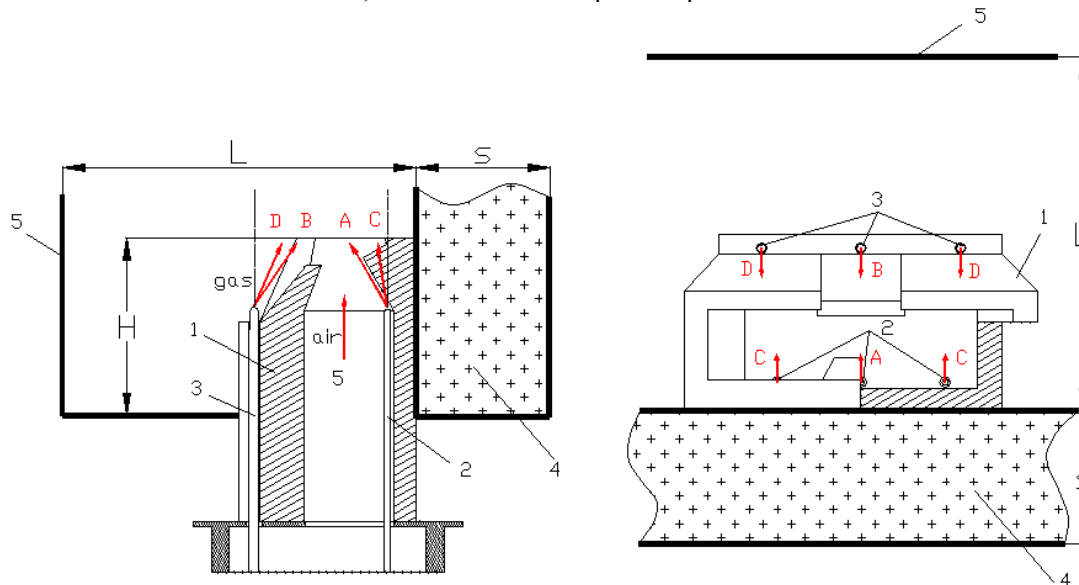


Figure 1. Furnace scheme. (1) burner refractory brick, (2) primary fuel-gas gun, (3) secondary fuel-gas gun, (4) furnace wall, and (5) furnace tube.

Table 1. Four flow categories.

Position	Flow name
Middle primary fuel-gas flow	Flow A
Middle secondary fuel-gas flow	Flow B
Lateral primary fuel-gas flow	Flow C
Lateral secondary fuel-gas flow	Flow D

The 6 fuel-gas flows from 6 fuel-gas guns can be classified into 4 categories, due to symmetry, in table 1.

The initial velocity directions of the 4 categories of flows are influenced by the shape of the burner refractory brick and fuel-gas guns, which of primary and secondary fuel-gas flows has opposite horizontal components. Flow A and Flow C, which are of the primary fuel-gas, are directed towards the furnace tube, whereas Flow B and Flow D, which are of secondary fuel-gas, are directed towards the furnace wall. Flow A and Flow B, which are in the middle, have initial velocities of larger angles to the vertical direction compared with Flow C and Flow D, which are on the sides.

The thickness of the furnace wall (s) is 0.3m. The furnace tube, which absorbs heat, is 1.2m away, (d), from the furnace wall. The height of the burner refractory brick (H) is 0.8m.

3. Numerical modelling

3.1. Numerical models and governing equations

The CFD software FLUENT 17.0 is used for finite element calculation and performs well for complex geometry and chemical reactions. The standard $k-\varepsilon$ model, which is semi-empirical and was proposed by Launder and Spalding [6], was adopted for turbulent flow; moreover, this model has been proven qualified for flow calculation in practical engineering. Combustion reaction was modelled by using the Probability Density Function [7], in which factors that affect chemical reaction rate, including temperature and mole fraction, are given by the Beta Function. Moreover, radiant heat transfer was modelled by the Discrete Ordinates (DO) radiation model, which solves the radiant transfer equation (RTE) for a finite number of discrete solid angles [7]. The DO model was proposed by Chui and Raithby [8] and Murthy and Mathur [9] generalized it to the unstructured mesh.

In this combustion model, the formation of pollutant CO is mainly influenced by the mole fraction of oxygen [7]. A low oxygen fraction leads to incomplete combustion, which comes with higher CO formation.

Pollutant NO has a relatively low fraction in the flow field, which can be presumed to be effect-free on the flow field. The NO transport equations, therefore, are based on the calculated flow field, which brings about less computation. In this study, the mechanisms of NO formation included thermal NO and prompt NO [7], that the triple bond in nitrogen molecule breaks in high temperature, the generation of which, nitrogen free radical, initiates subsequent reactions. A triple nitrogen bond has a high dissociated energy, and is usually considered to break at temperatures over 1800K. This step of reaction, therefore, is determinant in the formation rate of pollutant NO. Other than temperature, the mole fraction of oxygen, as a reactant, also affects NO formation. The coefficients adopted in thermal and prompt NO models are based on estimate values of Hanson and Salinmian [10] and De Soete[11]. NO reburning was considered based on model proposed by Kandamby et al [12].

3.2. Geometry

X, y, z directions and base levels are defined in table 2.

Table 2. Coordinate definition.

Coordinate	Direction	Base level
x	furnace wall \rightarrow furnace tube	surface of furnace wall
y	base on right-hand rule according to x, z direction	burner refractory brick symmetry
z	initial velocity direction of air in burner refractory brick	furnace bottom

Figure 2 illustrates the geometry of furnace. Considering the impact of heat transfer of furnace wall, the computational domain consists of both fluid zone and solid zone. The fluid zone measures $1.2\text{m} \times 2\text{m} \times 6\text{m}$, for the complete reaction, and the top of it narrows to $0.5\text{m} \times 1\text{m}$, so that the backflow can be eliminated. The shape of the solid zone remains in the same with the fluid zone in the y and z directions, and the length in the x direction is 0.3m.

3.3. Operating and boundary conditions

Primary and secondary fuel-gas have the same mole fraction, as shown in table 3.

Operating condition: The total mass flow rate of the primary and secondary fuel-gas is 18.0 g/s, which corresponds to a burner combustion power of 1.1 MW. The flow rates of the 3 primary fuel-gas guns are the same, and same with those of the secondary fuel-gas guns. The mass flow rate of each primary fuel-gas gun increases from 1.0 g/s to 3.0 g/s. Correspondingly, the mass flow rate of each secondary fuel-gas gun decreases from 5.0 g/s to 3.0 g/s. The span of the mass flow rate between the two conditions is 0.1 g/s, and the Coefficient of excess air is 1.2.

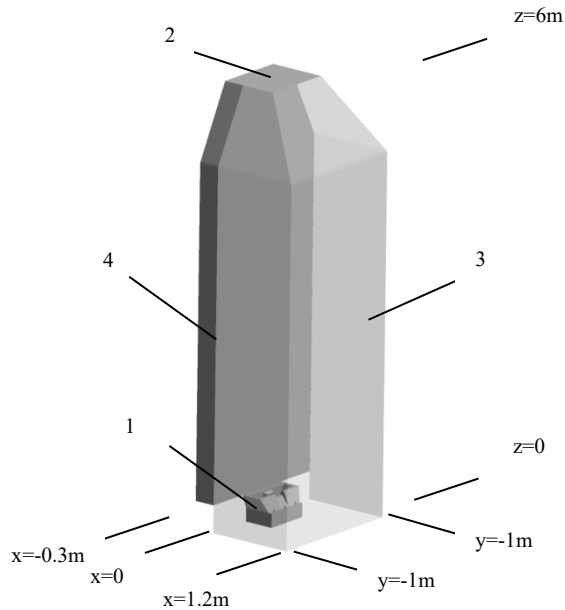


Figure 2. Geometry. (1) burner, (2) fluid zone outlet, (3) furnace tube surface, and (4) furnace wall, solid zone.

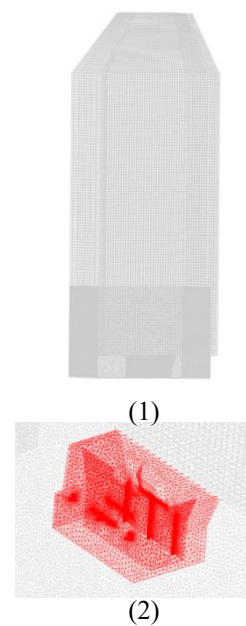


Figure 3. Mesh. (1) whole mesh, and (2) burner.

Table 3. Fuel-gas mole fraction.

Gas	H ₂	CH ₄	CO	C ₂ H ₄	C ₂ H ₆	C ₃ H ₈
Mole fraction	0.3794	0.6068	0.005	0.0065	0.0021	0.0002

The bottom of the burner refractory brick, as the inlet of air, and the bottoms of the 6 fuel-gas guns, as the fuel-gas inlet, are set as mass flow inlet. The outside surface of furnace wall is set to a constant temperature boundary of 300 K, corresponding to the practical temperature. The radiation emissivity of the inner surface of the furnace wall is set to 0.9. The tube surface, as the boundary of the fluid zone, is set to a constant temperature boundary of 1400K, corresponding to practical temperature of furnace gas. The top of fluid zone is set as constant pressure boundary of -60 Pa, corresponding to the practical pressure of furnace gas. Other surfaces, including those of the burner refractory brick and fuel-gas guns, are set as isothermal boundaries.

3.4. Mesh

The computational mesh is generated by ANSYS ICEM CFD 17.0, as shown in figure 3. The interior surface separates the fluid zone into two zones. The lower zone, which contains the burner refractory brick and fuel-gas nozzles, adopts tetrahedral cells to accommodate the anticipated large gradients of the variables, including temperature and fractions, in the flow field near furnace bottom. Hexahedra cells are applied in the upper fluid zone and the solid zone. The merged mesh (Mesh 1) consists of about 4,770,000 cells.

To test the mesh independence, Mesh 2 (with 3,850,000 cells) and Mesh 3 (with 2,930,000 cells) are established into the original geometry. The mass flow rate of each primary fuel-gas gun is 1.0 g/s, and that of the secondary is 5.0 g/s. Area-weighted average temperatures of the z axial cross sections in the three meshes are shown in figure 4.

In this operating condition, the computational result barely changes after the cell amount reaches 3,850,000. Meanwhile, Mesh 1, with about 4,770,000 cells, has more accurate computational results than Mesh 2. Mesh 1, therefore, was selected for subsequent computation.

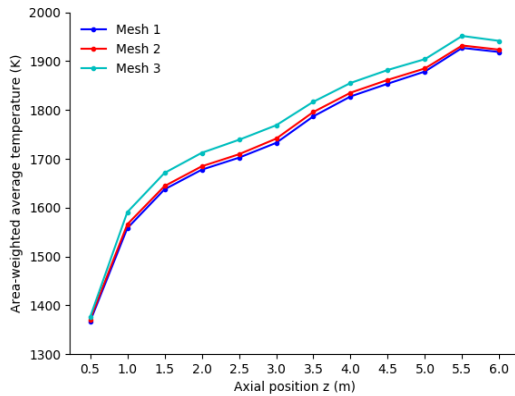


Figure 4. Area-weighted average temperature of z axial cross sections.

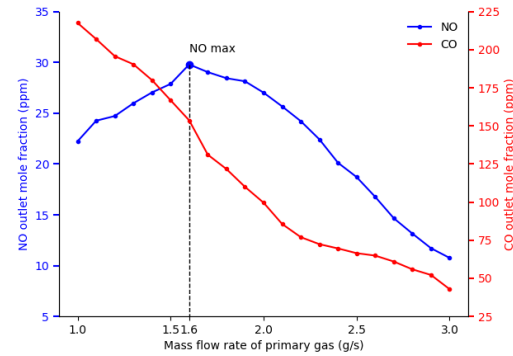


Figure 5. Outlet mole fraction of pollutants NO and CO of each operating condition.

4. Results analysis

Outlet mole fractions of the pollutant NO and CO, in each operating condition, are shown in figure 5.

In the computational interval, the outlet NO fraction peaks at 29.8 ppm when the mass flow rate of each primary fuel-gas gun is 1.6 g/s. Outlet CO fraction decreases with the increase of primary fuel-gas mass flow rate, from 217.5 ppm to 42.9 ppm.

Three representative operating conditions are defined in table 4. Respectively, Conditions 1 and 3 are conditions with smallest/largest primary fuel-gas flow rates. Condition 2 is the condition with the highest outlet NO fraction. The inlet pressure, to which inlet mass flow rate corresponds, of each operating condition meets the requirement of practical operation in petrochemical factories, ranging from about 15 kPa to 150 kPa.

Table 4. Definition of three representative operating conditions.

Mass flow rate/ pressure	Condition 1	Condition 2	Condition 3
Mass flow rate of each primary fuel-gas gun (g/s)	1.0	1.6	3.0
Inlet pressure of primary fuel-gas gun (kPa)	26.8	77.7	135.4
Mass flow rate of each secondary fuel-gas gun (g/s)	5.0	4.4	3.0
Inlet pressure of secondary fuel-gas gun (kPa)	98.5	65.3	21.1

4.1. Oxygen fraction field and formation of CO

On plane $y=0$, the oxygen mole fraction, velocity and pathlines of the 4 flows between plane $z=0$ and $z=2.0$ m are shown in figure 6. According to the distribution of pathlines, for Condition 1, which has the smallest primary fuel-gas flow rate, the primary Flows of A and C are influenced by the secondary Flows of B and D; moreover, all 4 pathlines of which stick to the inner surface of the furnace wall. For Conditions 2 and 3, as the primary fuel-gas flow rate increases, and when the secondary flow rate decreases, the pathlines of the middle Flows of A and B are deflected to the furnace tube gradually, whereas the pathlines of the lateral Flows of C and D, which stick to the inner surface of the furnace wall, are barely influenced by the changes in different operating conditions.

According to oxygen fraction distribution, for the 3 representative operating conditions, the region near burner refractory brick can be divided into 3 zones.

Zone 1- Inlet flow zone, with relatively high speed, which includes the primary and secondary fuel-gas flow and air flow.

Zone 2- Furnace tube swirling zone, including the furnace gas between Zone 1 and furnace tube. In this zone, the gas near the high-speed Zone 1 gas has the same velocity direction with Zone 1 gas, whereas the gas far away from Zone 1, which is near the furnace tube, has opposite velocity direction, which forms the swirling flow on a large scale.

Zone 3- Furnace wall swirling zone, including the furnace gas between Zone 1 and furnace wall. Similar to Zone 2, in Zone 3, the velocity of gas near Zone 1 is the same with that of Zone 1, whereas the velocity of gas far away from Zone 1, which is near furnace wall, is opposite from that of Zone 1, which forms the swirling flow zone on a smaller scale compared with that of Zone 2.

Due to 1.2 being the coefficient of excess air, the extra oxygen exists in the furnace gas of Zones 2 and 3. Zone 1, which consists of fuel-gas and oxygen, is the main domain where combustion takes place; therefore, the oxygen fraction of Zone 1 is relatively low and close to 0. For Condition 1, Flows of A, B, C and D are deflected to the furnace wall; Zone 3 is pressed to a small triangular area next to the furnace wall and the bottom of the furnace. The swirl in Zone 3 is on a small scale, with a low oxygen fraction. Correspondingly, the swirl in Zone 2 is large with a relatively high oxygen fraction. For Conditions 2 and 3, Zone 1 moves gradually towards the furnace tube, which leads to a smaller scale of Zone 2 with lower oxygen fraction. Correspondingly, Zone 3 scale increases, with increasing oxygen fraction. In Condition 3, the top of Zone 3 get connected to the plane $z=2.0$ m.

The furnace wall impedes the circulation of furnace gas in Zones 2 and 3. Zone 2, on a larger scale, is less effected by Zone 1, which has a greater effect on Zone 3 on a smaller scale. As the main combustion reaction area, the increasing scale of Zone 3, together with the increased oxygen fraction, influences the formation of pollutants CO and NO. From Condition 1 to Condition 3, the oxygen fraction in the combustion area increases gradually, leading to the decreasing outlet CO fraction.

4.2. Temperature field and NO formation rate

The temperature and NO formation rate on planes $z=1.0, 1.5, 2.0, 2.5$ and 3.0 m in Conditions 1, 2 and 3 are shown in figure 7. From Condition 1 to Condition 3, the middle Flows of A and B deflect towards the furnace tube; whereas the lateral Flows of C and D stick to the furnace wall, as reflected in the temperature field. For Conditions 1 and 2, as concluded in Section 4.1, the fuel-gas flow has not completely stuck to the furnace wall at the height $z=1.0$ m, leading to a relatively high oxygen fraction. This area, meanwhile, as the initial combustion area, has the strongest chemical reaction caused by the highest fuel-gas fraction, leading to the highest temperature. The temperature of the outer flame is higher than that of the inner flame, due to increased oxygen supply from furnace gas, thereby resulting in three circles at 1800 K-above region, as well as a high-NO formation rate region, corresponding to the 3 gas-fuel flows (including 1 middle flow and 2 lateral ones). For areas with z coordinate ranging from 0 to 1.0m, NO formation is dominated by temperature, which is reflected in, that areas with temperature above 1800K are mainly equals to areas with high formation rate of NO.

For areas with z coordinate > 1.0 m, the lateral fuel-gas Flows of C and D stick to the furnace wall, which results in the lateral flame sticking to the furnace wall, as well as the 1800 K-above region that the flame generates. The high-temperature region generated by the middle flame of fuel-gas Flows of A and B, changes with different operating conditions. The 1800 K-above in Condition 2 is of a slightly larger x axial scale, compared with Condition 1, resulting from the deflection to the furnace tube of the middle fuel-gas Flows of A and B. It is more obvious in Condition 3 that the 1800 K-above region on plane $z=1.5$ m is shaped in U-style, due to most degree of deflection of the middle Flows of A and B, which results in the separation of middle and lateral flame on x axis. Correspondingly, the scale of 1800 K-above region on the z axis decreases from Condition 1 to Condition 3, which is obviously reflected on planes $z=2.5$ and 3.0 m.

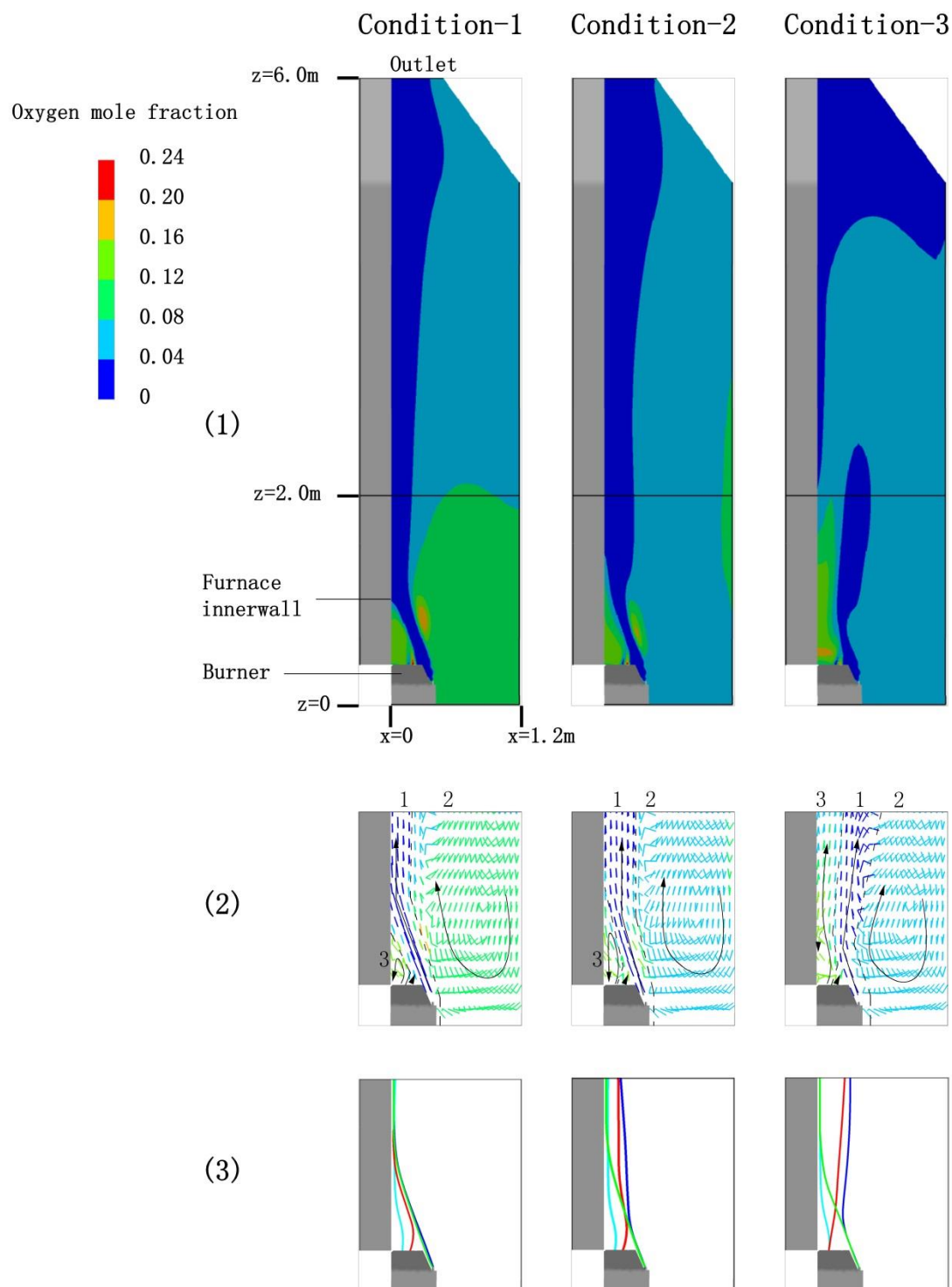


Figure 6. Oxygen mole fraction, velocity and pathline on plane $y=0$. (1) oxygen fraction, (2) velocity (1-inlet flow 2-furnace tube swirl 3-furnace wall swirl), and (3) pathline — Flow A — Flow B — Flow C — Flow D.

For Condition 3, areas with temperature above 1800 K are mainly equal to areas with a high formation rate of NO, similar to planes $z=1.0$ m in Conditions 1 and 2. As concluded in Section 4.1, Zone 3 has the largest scale in Condition 3, resulting in the highest oxygen fraction near the furnace wall, which is the main area of combustion reaction. NO formation is barely restrained by the ample supply of oxygen and is dominated by the temperature in Condition 3.

On planes $z=1.5$ and 2.0 m in Condition 1, NO is barely formed near the furnace wall, despite the temperature being above 1800 K. As concluded in Section 4.1, in the area near the furnace wall, oxygen fraction is the lowest, which restrains NO formation. For areas in Condition 1 with coordinates >1.0 m, therefore, NO formation is dominated by oxygen fraction.

Condition 2 is between Conditions 1 and 3 and closer to Condition 1. Areas on planes $z=1.5$ and 2.0 m exist with 1800 K-above temperature and low NO formation rate, which means that oxygen fraction dominates NO formation in these areas. Compared with low oxygen fraction in the combustion area caused by fuel-gas flow sticking to the furnace wall in Condition 1, and relatively low temperature in the combustion area caused by flame separation, the highest NO formation rate appears on plane $z=2.0$ m in Condition 2.

NO formation rate along the pathlines of fuel-gas Flow B is shown in figure 8, the integral of which can approximately reflect the outlet NO fraction. The NO formation of Condition 2, with the highest outlet NO fraction and largest integral area, peaks the highest, due to the large scale of 1800K-above area caused by the incomplete flame separation and high oxygen fraction in combustion area caused by the incomplete sticking to the furnace wall of fuel-gas Flows of A and B. The NO formation rate of Condition 3, with the lowest outlet NO fraction and largest integral area, peaks the lowest, which subsequently slumps to near zero rapidly, resulting from the relatively low combustion temperature caused by flame separation. The NO formation of Condition 1 lies between the other two, over Condition 3; therefore, we concluded that flame separation, for the reduction of combustion temperature, is a more effective approach for NO formation restraint than reduction of oxygen fraction in this study.

4.3. Uniformity of heat transfer on the furnace tube surface

Usually, in a furnace, heat is transferred to the receiver via convection of the furnace gas with high temperature. In this case, however, the flame sticks to the furnace wall, thereby heating the wall to a high temperature, and heat radiation becomes non-neglectable, as shown in figure 9.

The power of heat transfer on the furnace tube surface along the z axis in Conditions 1, 2 and 3 is shown in figure 10. From Condition 1 to Condition 3, as the flame deflects to the furnace tube, the heat radiation from furnace wall weakens, resulting in increased heat transfer to the furnace tube by convection. In Condition 3, where the flame is deflected the most to the furnace tube, the heat transfer power peaks at $z = 2.5$ m. For all three conditions, the temperature of furnace gas plateaus after the combustion reaction completely finishes. Therefore, the heat transfer power falls slowly after the peak, with the z coordinate increasing.

According to the sectional average temperature along the z axis in Section 3.4, the furnace gas temperature drops dramatically as the z coordinate decreases at $z < 2.0$ m, due to the incomplete combustion in this area, wherein the furnace gas is mainly from the upper swirl, leading to lower convection power compared with the area with high temperature. In Condition 1, which has the highest level of wall-sticking flame and highest power of wall radiation, the heat transferred to the furnace tube is relatively more uniform, as reflected in the weak trend that the heat transferred to the furnace tube decreases with the z coordinate. Condition 3, on the contrary, has a large difference on heat transfer between its peak and furnace bottom.

5. Conclusion

Separation of primary and secondary fuel-gases leads to flame separation, and this becomes obvious with increasing primary fuel-gas flow rate. Flame separation leads to a decreased 1800 K-above area, which further constrains NO formation, as concluded in Section 4.2.

The furnace wall impedes the circulation of furnace gas, resulting in a small swirling area, with a high oxygen fraction around the furnace wall. The swirling area increases with a high primary fuel-gas flow rate, thereby leading to an increased oxygen supply, which is conducive to lower CO outlet fraction and adverse to NO formation constraint, as concluded in Section 4.1 and 4.2.

The wall-sticking flame leads to non-neglectable heat radiation from the furnace wall to the tube, which increases with high primary flow rate and an increased level of wall-sticking flame. Moreover, the increased power of heat radiation results in improved heat transfer uniformity on the furnace tube, as concluded in Section 4.3.

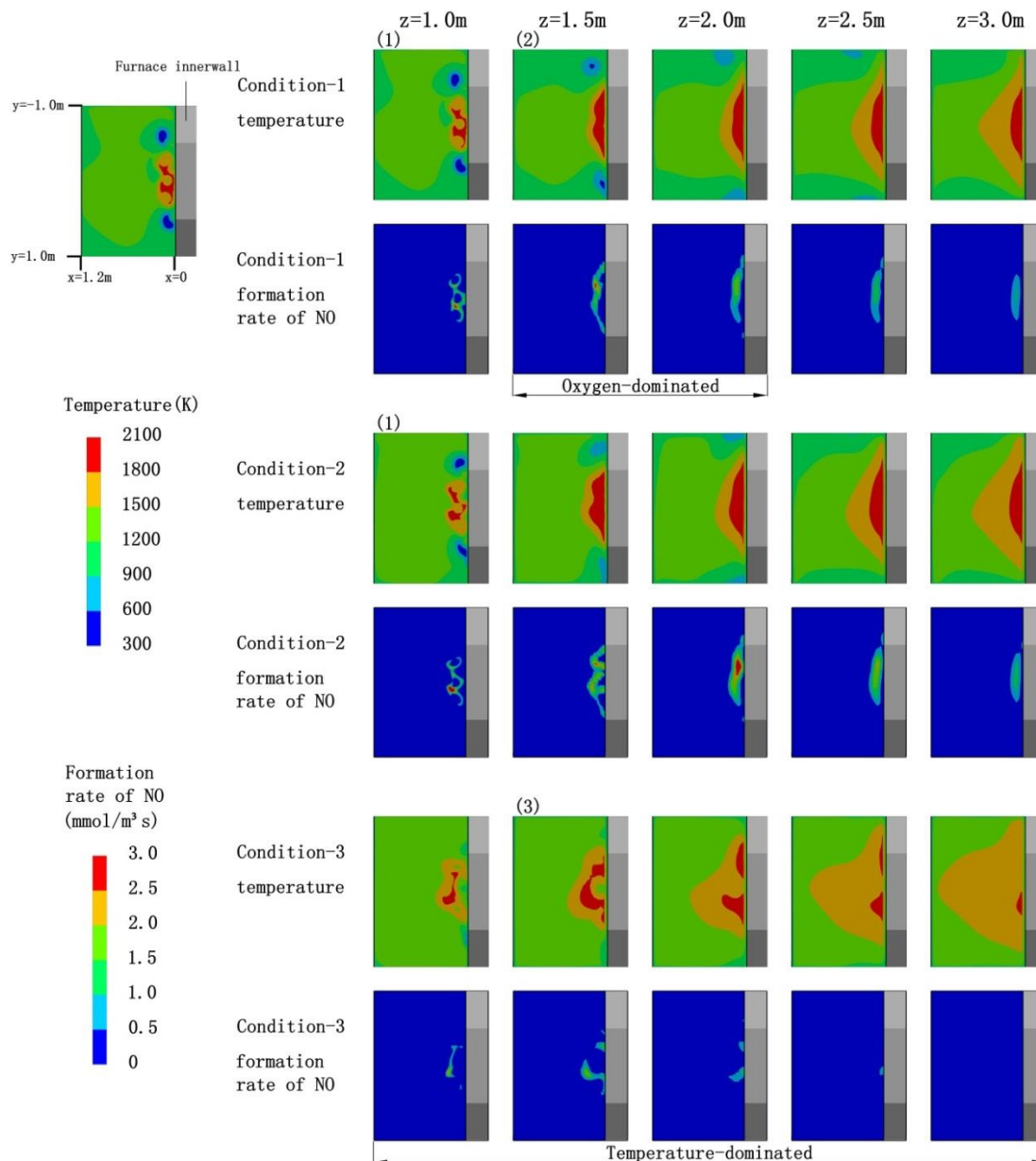


Figure 7. Temperature and NO formation rate on z axial cross sections. (1) three circles corresponding to three fuel-gas flows, (2) low NO formation rate near the furnace wall due to low oxygen fraction, and (3) low temperature due to flame separation, U-style.

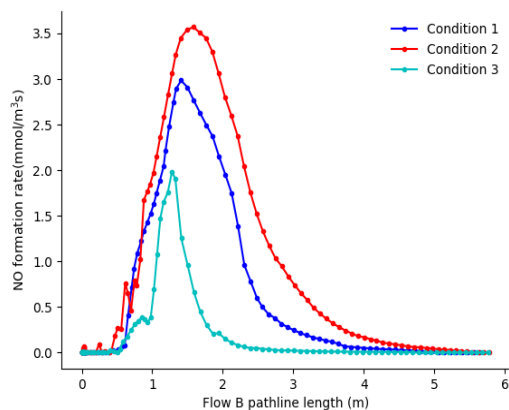


Figure 8. NO formation rate along pathline of Flow B.

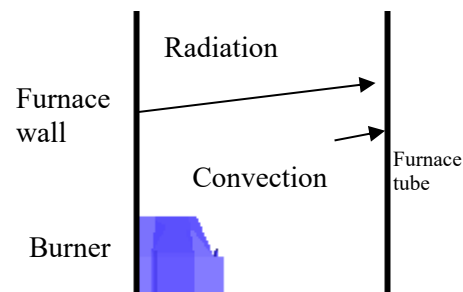


Figure 9. Two main approaches of heat transfer.

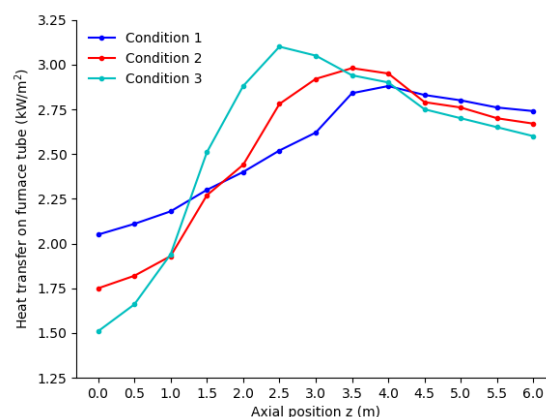


Figure 10. Power of heat transfer on tube surface along z axis.

References

- [1] S.C. Hill, L.D. Smoot, Modeling of nitrogen oxides formation and destruction in combustion systems[J]. Progress in Energy and Combustion Science, 2000, 26(4): 417-457.
- [2] J. Chacón, M. J. Sala, J. M. Blanco. Investigation on the design and optimization of a low NO_x-CO emission burner both experimentally and through computational fluid dynamics (CFD) simulations[J].
- [3] P. Bělohradský, V. Kermes, Experimental study on NO_x formation in gas-staged burner based on the design of experiments, Chem. Eng. Trans. 29 (2012) 79–84.
- [4] B. Liu, S. Wang, Y. Wang, et al. CFD study on air staged burner of tube furnace[J]. Acta Petrolei Sinica (Petroleum Processing Section), 2013, 29(6): 1040-1046.
- [5] GB31571-2015, Pollutant Discharge Standard of Petrochemical Industry[S].
- [6] B.E. Launder, D.B. Spalding, Lectures in Mathematical Models of Turbulence, Academic Press, London, England, 1972.
- [7] FLUENT 13.0 Help Documentation.
- [8] E.H. Chui, G.D. Raithby, Computation of radiant heat transfer on a nonorthogonal mesh using the finite-volume method, Numer. Heat Transfer, Part B 23 (1993) 269–288.

- [9] J.Y. Murthy, S.R. Mathur, Finite volume method for radiative heat transfer using unstructured meshes, AIAA (1998) 98–0860.
- [10] Y.R. Sivathanu, G.M. Faeth, Generalized state relationships for scalar properties in nonpremixed hydrocarbon/air flames, Combust. Flame 82 (1990) 211–230.
- [11] G.G. De Soete, Overall reaction rates of NO and N₂ formation from fuel nitrogen, in: 15th Symposium (International) on Combustion, The Combustion Institute, 1975, pp. 1093–1102.
- [12] N. Kandamby, G. Lazopoulos, F.C Lockwood, A. Perera, L. Vigevano, Mathematical Modeling of NO_x Emission Reduction by the Use of Reburn Technology in Utility Boilers, in: ASME Int. Joint Power Generation Conference and Exhibition, Houston, Texas, 1996.